Beating dark–dark solitons in Bose–Einstein condensates

2012 J. Phys. B: At. Mol. Opt. Phys. 45 115301

(http://iopscience.iop.org/0953-4075/45/11/115301)

J. Phys. B: At. Mol. Opt. Phys. **45** (2012) 115301 (11pp) doi:10.1088/0953-4075/45/11/115301

Beating dark–dark solitons in Bose–Einstein condensates

D Yan[1], J J Chang[2], C Hamner[2], M Hoefer[3], P G Kevrekidis[1], P Engels[2], V Achilleos[4], D J Frantzeskakis[4] and J Cuevas[5]

[1] Department of Mathematics and Statistics, University of Massachusetts, Amherst, MA 01003-4515, USA
[2] Washington State University, Department of Physics & Astronomy, Pullman, WA 99164, USA
[3] North Carolina State University, Department of Mathematics and Statistics, Raleigh, NC 27695, USA
[4] Department of Physics, University of Athens, Panepistimiopolis, Zografos, Athens 157 84, Greece
[5] Nonlinear Physics Group, Escuela Politécnica Superior, Departamento de Física Aplicada I, Universidad de Sevilla, C/ Virgen de África, 7, 41011-Sevilla, Spain

E-mail: yan@math.umass.edu and kevrekid@math.umass.edu

Received 2 February 2012, in final form 29 March 2012
Published 18 May 2012
Online at stacks.iop.org/JPhysB/45/115301

Abstract
Motivated by recent experimental results, we study beating dark–dark (DD) solitons as a prototypical coherent structure that emerges in two-component Bose–Einstein condensates. We showcase their connection to dark–bright solitons via $SO(2)$ rotation, and infer from it both their intrinsic beating frequency and their frequency of oscillation inside a parabolic trap. We identify them as exact periodic orbits in the Manakov limit of equal inter- and intra-species nonlinearity strengths with and without the trap and showcase the persistence of such states upon weak deviations from this limit. We also consider large deviations from the Manakov limit illustrating that this breathing state may be broken apart into dark–anti-dark soliton states. Finally, we consider the dynamics and interactions of two beating DD solitons in the absence and in the presence of the trap, inferring their typically repulsive interaction.

(Some figures may appear in colour only in the online journal)

1. Introduction

One of the principal themes of study in the emerging field of atomic Bose–Einstein condensates (BECs) is the examination of the coherent structures that arise in them [1–4]. When such explorations started over a decade ago [5–9], they were considerably hindered by either geometric or thermal effects, which were detrimental towards the lifetime of dark solitons and vortices that can be formed in repulsive BECs. Yet, the newer generations of experiments have enabled considerable strides towards the observation of dynamics and interactions of such nonlinear waveforms [10–15].

In addition to the above context of single-component BECs, soliton and vortex states may also arise in multi-component condensates, such as the two-component pseudo-spinor BECs, or the three-component and higher component spinor BECs [1, 2, 4]. One of the prototypical examples of a soliton state in these settings is the so-called dark–bright (DB) soliton [16, 17]. Experimental images of DB solitons in a two-component BEC are presented in figure 1. The BEC in this figure is comprised of two different hyperfine states of ^{87}Rb, and the solitons are generated by subjecting the BEC to inter-component counterflow; details of this technique are described in [18, 19]. In each panel, the atom clouds of the two components are vertically offset for imaging only, while all the dynamics leading to the soliton formation occurs in overlapped clouds. Clear examples of DB solitons are marked as 'DB' in the figure and they consist of a dark soliton in one component that is coupled to a bright soliton in the second component. These structures can be thought of as 'symbiotic' (or even parasitic) states because their bright component cannot be supported alone in the case of repulsive interactions [3]; in fact, the bright soliton is only sustained because of the presence of its dark counterpart, which operates as an external trapping potential. Although DB solitons (and even a prototypical interaction thereof) were first observed some time ago in the context of nonlinear optics [20, 21], their observation in recent atomic BEC experiments [10] triggered

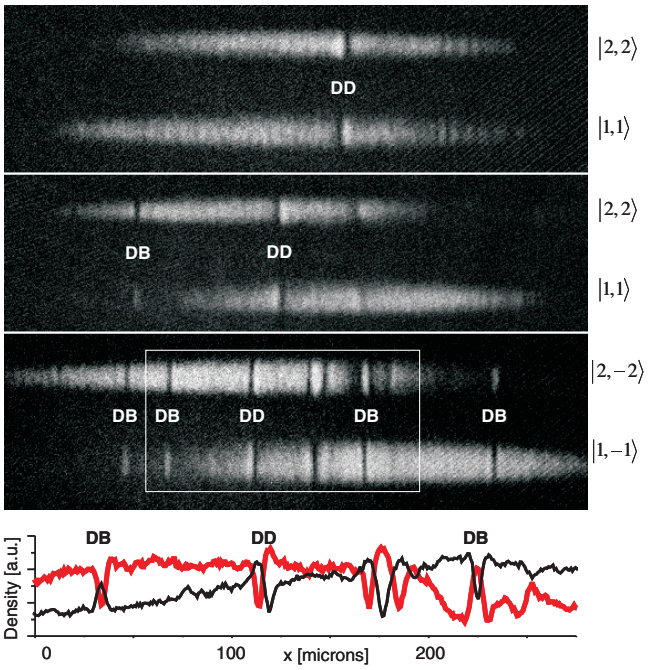

Figure 1. Prototypical experimental images of dark–bright and dark–dark solitons in a two-component BEC. The two components are vertically offset for separate imaging. All dynamics occur with vertically overlapped components before the imaging procedure. Clear examples of dark–bright and dark–dark solitons are marked as DB and DD, respectively. In the fourth panel, the red (thick) line shows a radially integrated cross section of the upper component in the boxed region of the third panel, while the black (thin) line shows the cross section of the lower component. The $|F, m_F\rangle$ hyperfine states used for these images are given to the right of each component.

a sizeable burst of research activity centred around them. Topics of study included (but were not limited to) multi-DB soliton solutions from the viewpoint of integrable systems [22], numerical study of DB soliton interactions [23], discrete DB solitons [24], experimental realizations of DB soliton trains [18], DB soliton oscillations and interactions [25, 26] as well as interaction of DB solitons with localized impurities [27].

Recently, a 'cousin' of these DB solitons, namely the dark–dark (DD) soliton—which involves two dark solitons but with potentially a breathing oscillation between their densities was also experimentally observed [19]. Pertinent examples are marked as 'DD' in figure 1. These solitons show interesting dynamics in which they periodically change their form, from the one shown in the first panel to the one shown in the second panel and back (note the order of the hump/notch features in each of the DD components; see also figure 5 below). Such 'beating DD solitons' are expected to emerge in the integrable two-component (so-called Manakov) limit of the relevant mean-field theoretic models [28] and were, in fact, earlier observed in numerical experiments involving the dragging of defects through the binary condensates [29].

The current experimental advances, such as the ones leading to the soliton images of figure 1, motivate the present theoretical study, in which we revisit DD soliton states at the integrable Manakov limit and extract information from their connection to the DB solitons (section 2). These results are corroborated by the identification of such single-DD soliton states, as genuine periodic orbits of the Manakov case (with and without a trap) and the study of their stability, internal modes and associated near-equilibrium dynamics (section 3). In addition, we examine the dynamics of such individual solitons upon departure from the integrable limit (section 4). Experimentally it has also become possible to generate several solitons, and even solitons of different types, in a single BEC—see, e.g., the third panel of figure 1 which demonstrates the coexistence of DB and DD solitons. Although the experimentally exploited counterflow between the two components is beyond the scope of our current analysis, these experimental findings motivate our investigation of the interactions between two DD solitons (section 5). Finally, conclusions of our study, as well as a number of interesting perspectives for future work, are also presented (section 6).

2. DB and DD solitons: theoretical background

We consider a two-component elongated (along the x-direction) repulsive BEC, composed of two different hyperfine states of the same alkali isotope. In the case of a highly anisotropic trap (i.e. if the longitudinal and transverse trapping frequencies are such that $\omega_x \ll \omega_\perp$), this system can be described by two coupled Gross–Pitaevskii equations (GPEs) of the form [1]:

$$\mathrm{i}\,\hbar\partial_t\psi_j = \left(-\frac{\hbar^2}{2m}\partial_x^2\psi_j + V(x) - \mu_j + \sum_{k=1}^{2} g_{jk}|\psi_k|^2\right)\psi_j. \quad (1)$$

Here, $\psi_j(x,t)$ $(j=1,2)$ denote the mean-field wavefunctions of the two components (normalized to the numbers of atoms $N_j = \int_{-\infty}^{+\infty}|\psi_j|^2\mathrm{d}x$), m is the atomic mass, and μ_j are the chemical potentials; furthermore, $g_{jk} = 2\hbar\omega_\perp a_{jk}$ are the effective one-dimensional (1D) coupling constants, a_{jk} denote the three s-wave scattering lengths (note that $a_{12} = a_{21}$) which account for collisions between atoms belonging to the same (a_{jj}) or different (a_{jk}, $j \neq k$) species, while $V(x) = (1/2)m\omega_x^2x^2$ is the external trapping potential.

Let us now assume that the two-component BEC under consideration consists of two different hyperfine states of ^{87}Rb, such as the states $|1,-1\rangle$ and $|2,1\rangle$ used in the experiment of [30], or the states $|1,-1\rangle$ and $|2,-2\rangle$ used in the experiments of [18, 25, 19]. In the first case, the scattering lengths take the values $a_{11} = 100.4a_0$, $a_{12} = 97.66a_0$ and $a_{22} = 95.00a_0$, while in the second case, the respective values are $a_{11} = 100.4a_0$, $a_{12} = 98.98a_0$ and $a_{22} = 98.98a_0$ (where a_0 is the Bohr radius). In either case, it is clear that the scattering lengths take approximately the same values, say $a_{ij} \approx a$. This way, measuring the densities $|\psi_j|^2$, length, time and energy in units of $2a$, $a_\perp = \sqrt{\hbar/\omega_\perp}$, $\omega_\perp^{-1}$ and $\hbar\omega_\perp$, respectively, we may cast equations (1) into the following dimensionless form:

$$\mathrm{i}\partial_t u_1 = -\tfrac{1}{2}\partial_x^2 u_1 + V(x)u_1 + (|u_1|^2 + |u_2|^2 - \mu)u_1, \quad (2)$$

$$\mathrm{i}\partial_t u_2 = -\tfrac{1}{2}\partial_x^2 u_2 + V(x)u_2 + (|u_1|^2 + |u_2|^2 - \mu)u_2, \quad (3)$$

where we have also assumed that the chemical potentials characterizing each component are equal. Note that the potential in equations (2) and (3) is now given by $V(x) =$

$(1/2)\Omega^2 x^2$, where $\Omega = \omega_x/\omega_\perp$ is a natural small parameter of the system.

The above system of equations (2) and (3) is invariant under $SU(2)$ rotations [28]. In particular, let us first recall that a general matrix element of $SU(2)$ takes the form

$$U = \begin{pmatrix} \alpha & -\beta^* \\ \beta & \alpha^* \end{pmatrix},$$

where α and β are complex constants such that $|\alpha|^2+|\beta|^2 = 1$. Then, it can be shown that if $(u_1, u_2)^T$ are solutions of equations (2) and (3), then,

$$\begin{pmatrix} u_1' \\ u_2' \end{pmatrix} \equiv U \begin{pmatrix} u_1 \\ u_2 \end{pmatrix} = \begin{pmatrix} \alpha u_1 - \beta^* u_2 \\ \beta u_1 + \alpha^* u_2 \end{pmatrix},$$

are also the solutions of equations (2) and (3). This suggests that we may start from the exact DB soliton solution (which exists in the absence of the potential) and derive the beating DD soliton solution. More specifically, in the absence of the external potential ($V(x) = 0$) and for the boundary conditions $|u_1|^2 \to \mu$ and $|u_2|^2 \to 0$ as $|x| \to \infty$, equations (2) and (3) possess an exact analytical single-DB soliton solution of the following form:

$$u_1(x,t) = \sqrt{\mu}\{\cos\phi \tanh\xi + \mathrm{i}\,\sin\phi\}, \tag{4}$$

$$u_2(x,t) = \eta\,\mathrm{sech}\,\xi\,\exp\{\mathrm{i}\,kx + \mathrm{i}\,\theta(t)\}, \tag{5}$$

where $\xi = D(x - x_0(t))$, ϕ is the dark soliton's phase angle, $\cos\phi$ and η represent the amplitude of the dark and bright solitons, and D and $x_0(t)$ are associated with the inverse width and the centre position of the DB soliton. Furthermore, $k = D\tan\phi$ and $\theta(t)$ are the (constant) wavenumber and phase of the bright soliton, respectively. The above parameters of the DB soliton are connected through the following equations:

$$D^2 = \mu\cos^2\phi - \eta^2, \tag{6}$$

$$\dot{x}_0 = k = D\tan\phi, \tag{7}$$

$$\dot{\theta} = \tfrac{1}{2}(D^2 - k^2), \tag{8}$$

with $\dot{x}_0$ and $\dot{\theta}$ denoting the DB soliton velocity and angular frequency, respectively (overdots denote time derivatives). Thus, the DB solitons (4) and (5) are characterized by three free parameters (seven parameters $\mu, \phi, \eta, k, D, \dot{x}_0, \dot{\theta}$ and four constraints (6)–(8)). Note that the amplitude η of the bright soliton, the chemical potential μ of the dark soliton and the (inverse) width parameter D of the DB soliton are connected to the number of atoms N_B of the bright soliton by means of the following equation:

$$N_B \equiv \int_{\mathbb{R}} |u_2|^2\,\mathrm{d}x = \frac{2\sqrt{\mu}\eta^2}{D}. \tag{9}$$

According to the above arguments, one may start from the DB soliton and construct $SU(2)$-rotated solutions, in the following form:

$$u_1(x,t) = \alpha\sqrt{\mu}\{\cos\phi\tanh\xi + \mathrm{i}\,\sin\phi\} - \beta^*\eta\,\mathrm{sech}\,\xi\,\exp\{\mathrm{i}\,kx + \mathrm{i}\,\theta(t)\}, \tag{10}$$

$$u_2(x,t) = \beta\sqrt{\mu}\{\cos\phi\tanh\xi + \mathrm{i}\,\sin\phi\} + \alpha^*\eta\,\mathrm{sech}\,\xi\,\exp\{\mathrm{i}\,kx + \mathrm{i}\,\theta(t)\}. \tag{11}$$

With the additional four parameters $\alpha, \beta \in \mathbb{C}$ and the constraint $|\alpha|^2 + |\beta|^2 = 1$, the solutions (10) and (11) are characterized by six free parameters. Introducing a new parameter c, the velocity of the background fluid, another solution can be constructed from equations (10) and (11) via a Galilean boost: $\exp[\mathrm{i}\,(cx - c^2t/2)]u_{1,2}(x - ct, t)$. Thus, in the most general case, this DD soliton solution is characterized by seven free parameters. One natural set of parameters can be found from the far-field $|x| \to \infty$ behaviour consisting of two densities, an overall fluid velocity and four phases.

Due to Galilean invariance and phase invariance, $u_j'(x,t) = \mathrm{e}^{\mathrm{i}\varphi_j}u_j(x,t)$, we will assume, without loss of generality, that the background is at rest ($c = 0$) and focus, more specifically, on the case of the $SO(2)$-rotated DB soliton. In this case, the corresponding orthogonal matrix is given by

$$U = \begin{pmatrix} \cos(\chi) & -\sin(\chi) \\ \sin(\chi) & \cos(\chi) \end{pmatrix}, \tag{12}$$

where χ is an arbitrary angle. This way, the relevant $SO(2)$-rotated soliton solution takes the form

$$u_1(x,t) = \cos(\chi)\sqrt{\mu}\{\cos\phi\tanh(D(x - x_0(t))) + \mathrm{i}\,\sin\phi\} - \sin(\chi)\eta\,\mathrm{sech}(D(x - x_0(t)))\exp\{\mathrm{i}\,kx + \mathrm{i}\,\theta(t)\}, \tag{13}$$

$$u_2(x,t) = \sin(\chi)\sqrt{\mu}\{\cos\phi\tanh(D(x - x_0(t))) + \mathrm{i}\,\sin\phi\} + \cos(\chi)\eta\,\mathrm{sech}(D(x - x_0(t)))\exp\{\mathrm{i}\,kx + \mathrm{i}\,\theta(t)\}, \tag{14}$$

Solutions (13) and (14) are the DD soliton solutions characterized by four free parameters. The asymptotics of these solutions are $|u_1|^2 \to \mu\cos^2(\chi)$ and $|u_2|^2 \to \mu\sin^2(\chi)$ as $|x| \to \infty$. The densities of the above dark solitons read

$$n_1 \equiv |u_1|^2 = \mu\cos^2(\chi) - (\mu\cos^2(\chi)\cos^2\phi - \eta^2\sin^2(\chi)) \times \mathrm{sech}^2\xi - \sqrt{\mu}\eta\sin(2\chi)\{\sin\phi\sin[kx + \theta(t)] + \cos\phi\cos[kx + \theta(t)]\tanh\xi\}\,\mathrm{sech}\,\xi, \tag{15}$$

$$n_2 \equiv |u_2|^2 = \mu\sin^2(\chi) - (\mu\sin^2(\chi)\cos^2\phi - \eta^2\cos^2(\chi)) \times \mathrm{sech}^2\xi + \sqrt{\mu}\eta\sin(2\chi)\{\sin\phi\sin[kx + \theta(t)] + \cos\phi\cos[kx + \theta(t)]\tanh\xi\}\,\mathrm{sech}\,\xi, \tag{16}$$

while the total density n_{tot} of the DD soliton is given by

$$n_{\mathrm{tot}} = n_1 + n_2 = \mu - D^2\,\mathrm{sech}^2\xi. \tag{17}$$

Note that the total density of the DD soliton is time independent and has the form of a dark soliton density of depth D^2 on top of a background density μ. The above density is, in fact, identical to the density of the DB soliton; this is due to the fact that under $SO(2)$ rotation the total density, as well as all other conserved quantities of the system, remains unchanged. This will be particularly important when considering the motion of the DD soliton in a trap—see below.

On the other hand, one may consider the individual dark soliton densities, n_1 and n_2, across the trajectory of the DD

soliton, i.e. for $\xi = 0$: in such a case, $x = x_0(t) = kt$ and the densities read

$$n_1(\xi = 0) = \mu\cos^2(\chi)\sin^2\phi + \eta^2\sin^2(\chi) - \sqrt{\mu}\eta\sin(2\chi)\sin\phi\sin\left[\frac{1}{2}(k^2+D^2)t\right], \quad (18)$$

$$n_2(\xi = 0) = \mu\sin^2(\chi)\sin^2\phi + \eta^2\cos^2(\chi) + \sqrt{\mu}\eta\sin(2\chi)\sin\phi\sin\left[\frac{1}{2}(k^2+D^2)t\right]. \quad (19)$$

It is clear that $n_{1,2}(\xi = 0)$ are periodic functions of time; the relevant angular frequency (which constitutes the internal beating frequency of the DD soliton) is given by

$$\omega_0 = \tfrac{1}{2}(k^2+D^2) = \tfrac{1}{2}(\mu - \eta^2\sec^2\phi), \quad (20)$$

where we have also used equation (6). The frequency ω_0 is bounded by two limiting values. First, in the case $\eta \to 0$, the beating DD soliton becomes a stationary (in its density profile) DD soliton, characterized by a width $D = \sqrt{\mu}\cos\phi$ and a velocity $k = \sqrt{\mu}\sin\phi$; in this case, $\omega_0 \to (1/2)\mu$. Second, in the limiting case $D \to 0$, the beating DD soliton is reduced to a plane wave; in this case, $\omega_0 \to (1/2)k^2$. In other words, the intrinsic oscillation frequency takes values in the range

$$\tfrac{1}{2}k^2 < \omega_0 < \tfrac{1}{2}\mu. \quad (21)$$

3. DD solitons as periodic orbits in the Manakov model

In this section, we analyse the existence, stability and dynamics of single-beating DD solitons in a trap of the form $V(x) = \frac{1}{2}\Omega^2x^2$, considering them as periodic orbits. In the presence of the trap, the dynamics of the centre of mass $x_0(t)$ of the beating DD soliton is still described by the dynamics of the original (unrotated) DB soliton centre x_0. This is due to the fact that the GPEs (2, 3) are invariant under $SO(2)$ rotations even in the presence of $V(x)$, and so are all conserved quantities of the system, such as the total energy. Since the derivation of the equation of motion for the DB soliton centre x_0 in [16] was relying on the change of energy (due to the presence of the trap), it is clear that the evolution of the beating DD soliton centre follows the same dynamics: it performs a harmonic oscillation in the trap according to the equation $\ddot{x}_0 + \omega_{\rm osc}^2 x_0 = 0$, where the oscillation frequency $\omega_{\rm osc}$ is given by [16]

$$\omega_{\rm osc}^2 = \Omega^2\left(\frac{1}{2} - \frac{r}{8\sqrt{1+(\frac{r}{4})^2}}\right), \quad (22)$$

where $r = \frac{N_B}{\sqrt{\mu}}$ is a measure of the ratio of the number of atoms in the bright and dark soliton components. In order to compute the soliton profile and determine its stability, we consider the solutions of equations (2) and (3), with $g_{11} = g_{22} = g_{12} = 1$, as a Fourier series expansion of period ω_0[6], namely

$$u_1(x,t) = \sum_{k=-\infty}^{\infty} z_k(x)\mathrm{e}^{\mathrm{i}k\omega_0 t}, \quad u_2(x,t) = \sum_{k=-\infty}^{\infty} y_k(x)\mathrm{e}^{\mathrm{i}k\omega_0 t}, \quad (23)$$

with $\{z_k\}, \{y_k\} \in \mathbb{R}$. Then, the dynamical equations are reduced to a set of coupled equations:

$$[\mu - k\omega_0 - V(x)]z_k + \frac{1}{2}\partial_x^2 z_k = \sum_p\sum_q \left(z_p z_q^* + y_p y_q^*\right)z_{k-p+q}, \quad (24)$$

$$[\mu - k\omega_0 - V(x)]y_k + \frac{1}{2}\partial_x^2 y_k = \sum_p\sum_q \left(z_p z_q^* + y_p y_q^*\right)y_{k-p+q}, \quad (25)$$

where we have used the notation $z_k \equiv z_k(x)$, $y_k \equiv y_k(x)$. If the trap is absent, it is straightforward to see that the waveform of (23) with

$$z_0(x) = \sqrt{\frac{\mu}{2}}\tanh(\sqrt{2\omega_0}x) = y_0(x), \quad (26)$$

$$z_1(x) = -\sqrt{\frac{\mu}{2} - \omega_0}\,\mathrm{sech}(\sqrt{2\omega_0}x) = -y_1(x), \quad (27)$$

$$z_j(x) = y_j(x) = 0, \quad |j| > 1 \quad \text{or} \quad j = -1, \quad (28)$$

is actually the solution (13, 14) for $\chi = \pi/4$, $\phi = k = 0$ and $\omega_0 = D^2/2$. In order to numerically find a DD soliton solution in the system with the trap, the previous solution with the dark component $\{z_k\}$ multiplied by the Thomas–Fermi cloud with $u_1^{\rm TF} = \sqrt{\max(\mu - V(x), 0)}$ is introduced as a seed for a fixed-point method in the system of equations (24) and (25). Throughout this section, we have considered—for convenience—a trap strength $\Omega = 0.2$ in order to consume less time in the numerical calculations, as will be explained below. Figures 2 and 3 show the periodic orbit for $t = 0$ without and with a trap potential, respectively. It is worth remarking that solutions in the trap exist for $\mu > 2\omega_0$, as predicted in the end of section 2.

The choice of a trap strength $\Omega = 0.2$ for studying the stability of periodic orbits instead of, e.g., a value such as $\Omega = 0.01$ (which would represent a ratio of trap strengths much closer to a 1D situation) is twofold. On the one hand, as indicated by equation (22), the oscillation period scales with Ω^{-1}; consequently, decreasing 20 times the trap strength implies an integration time 20 times larger (for the same temporal resolution); on the other hand, the Thomas–Fermi radius ($R_{\rm TF} = \sqrt{2\mu}/\Omega$), which measures the condensate size would also increase 20 times, so the number of equations to integrate also increases in this way (at least for the same spatial resolution).

Once a periodic solution is found, its (linear) orbital stability can be analysed by means of Floquet analysis. To this end, the time evolution of a small perturbation $\{\xi_1(x,t), \xi_2(x,t)\}$ to a periodic solution $\{u_{1,0}(x,t), u_{2,0}(x,t)\}$ must be traced. For the double indices of $u_{i,j}$, i represents the component index, i.e. $i = 1, 2$ is the first and second components of the DD soliton solution respectively. The index $j = 0$ denotes that this is the (numerically) exact periodic solution for u_1 and u_2, around which we linearize in our Floquet

[6] Note that we cannot do this analysis for systems with $g_{11} : g_{12} : g_{22} \neq 1$ as, in that case, there is always an oscillation of the centre of mass (alike to that of a particle in a well) with a frequency non-commensurable to the beating frequency. Consequently, purely periodic orbits do not generically exist.

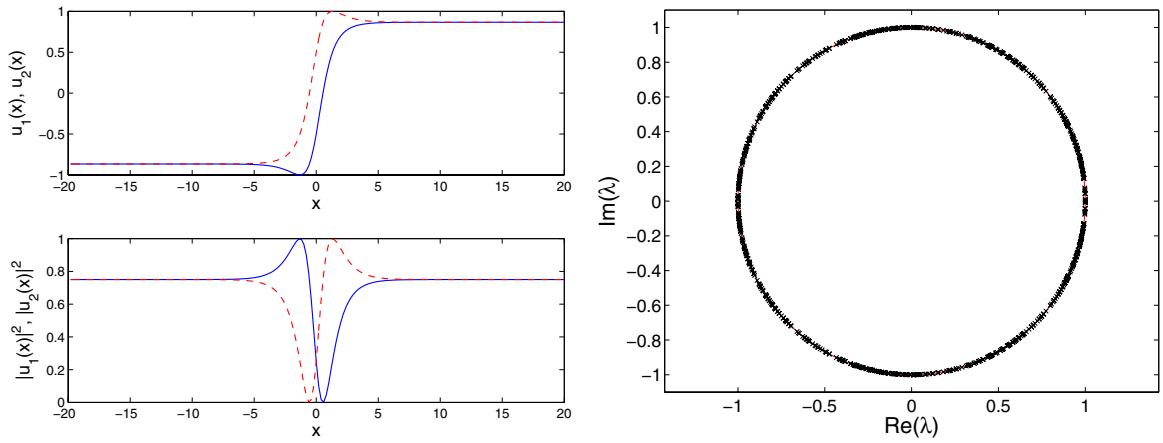

Figure 2. Left panel: profiles and densities of the beating DD soliton solution with $\Omega = 0$, $\omega_0 = 0.5$ and $\mu = 1.5$ at $t = 0$. Right panel: the Floquet multiplier spectrum for the DD soliton displayed in the left panel.

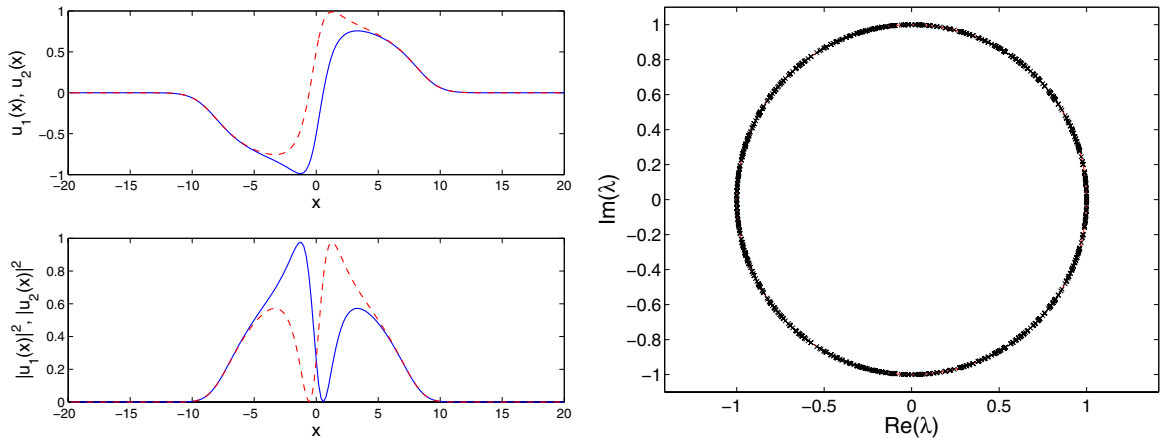

Figure 3. Same as figure 2 but in the trapped case with $\Omega = 0.2$.

analysis. The perturbations are introduced in the dynamical equations ((2) and (3)) as

$$u_1(x,t) = [u_{1,0}(x,t) + \delta\xi_1(x,t)],$$
$$u_2(x,t) = [u_{2,0}(x,t) + \delta\xi_2(x,t)], \tag{29}$$

and the resulting equation at order $O(\delta)$ reads

$$\mathrm{i}\,\partial_t\xi_1 = [-\tfrac{1}{2}\partial_x^2 + 2|u_{1,0}|^2 + |u_{2,0}|^2 - \mu + V(x)]\xi_1 + u_{1,0}^2\xi_1^* + u_{2,0}^*u_{1,0}\xi_2 + u_{2,0}u_{1,0}\xi_2^*, \tag{30}$$

$$\mathrm{i}\,\partial_t\xi_2 = [-\tfrac{1}{2}\partial_x^2 + |u_{1,0}|^2 + 2|u_{2,0}|^2 - \mu + V(x)]\xi_2 + u_{2,0}^2\xi_2^* + u_{1,0}^*u_{2,0}\xi_1 + u_{1,0}u_{2,0}\xi_1^*. \tag{31}$$

Then, in the framework of Floquet analysis, the stability properties of periodic orbits are resolved by diagonalizing the monodromy matrix $\mathcal{M}$, which is defined as

$$\begin{bmatrix} \mathrm{Re}(\xi_1(x,T)) \\ \mathrm{Im}(\xi_1(x,T)) \\ \mathrm{Re}(\xi_2(x,T)) \\ \mathrm{Im}(\xi_2(x,T)) \end{bmatrix} = \mathcal{M} \begin{bmatrix} \mathrm{Re}(\xi_1(x,0)) \\ \mathrm{Im}(\xi_1(x,0)) \\ \mathrm{Re}(\xi_2(x,0)) \\ \mathrm{Im}(\xi_2(x,0)) \end{bmatrix}, \tag{32}$$

with $T = 2\pi/\omega_0$. As the system is symplectic and Hamiltonian, the linear stability of the solutions requires that the monodromy eigenvalues λ (also called Floquet multipliers) must lie on the unit circle (see, e.g., [34, 35] for details). The Floquet multipliers can also be written as $\lambda = \exp(\mathrm{i}\,\Theta)$, with Θ denoting the Floquet exponent. An internal mode of the soliton corresponds to a spatially localized solution of equations (30) and (31), with its oscillation frequency related to the Floquet exponents as $\omega_\mathrm{m} = \Theta\omega_0/(2\pi)$. Figures 2 and 3 show a typical Floquet multiplier spectrum, indicating stability of the periodic orbits. All the analysed solutions (i.e. with $\Omega = 0$ and $\Omega = 0.2$) are stable.

Some interesting results can be extracted by the analysis of the internal modes of the periodic orbits. Figure 4(left) shows the dependence of three internal modes of the Floquet spectrum with respect to μ for $\omega_0 = 0.5$. The blue line is close to the frequency predicted by equation (22) (depicted as a dashed red line). Indeed, perturbing the beating DD soliton with the corresponding eigenmode, we have confirmed that this perturbation leads to an oscillation of the soliton in the trap with a frequency equal to that of the eigenmode (cf left panel of figure 5). It can be observed that the agreement between the numerical eigenfrequency and that predicted by equation (22) improves when μ increases, as expected. More specifically, the assumption that the solitary wave is a particle inside a Thomas–Fermi cloud is one of increasing validity the deeper one is within the Thomas–Fermi limit of large μ. The right panel of figure 4 shows the dependence of the frequency of

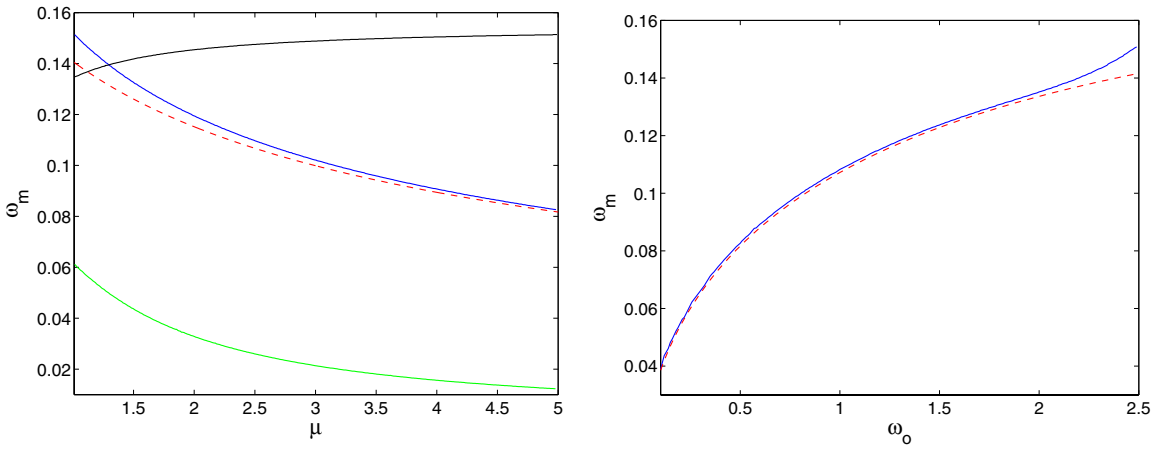

Figure 4. Left panel: dependence of the eigenfrequencies of some internal modes (solid lines) with respect to μ with fixed $\omega_0 = 0.5$ (the black, blue, green and red lines are the upper solid, middle solid, lower solid and the dashed respectively). Right panel: the dependence with respect to ω_0 with fixed $\mu = 5$ for the mode in blue in the left panel. In both panels, the red dashed line corresponds to the oscillation frequency (22) in a trap with $\Omega = 0.2$.

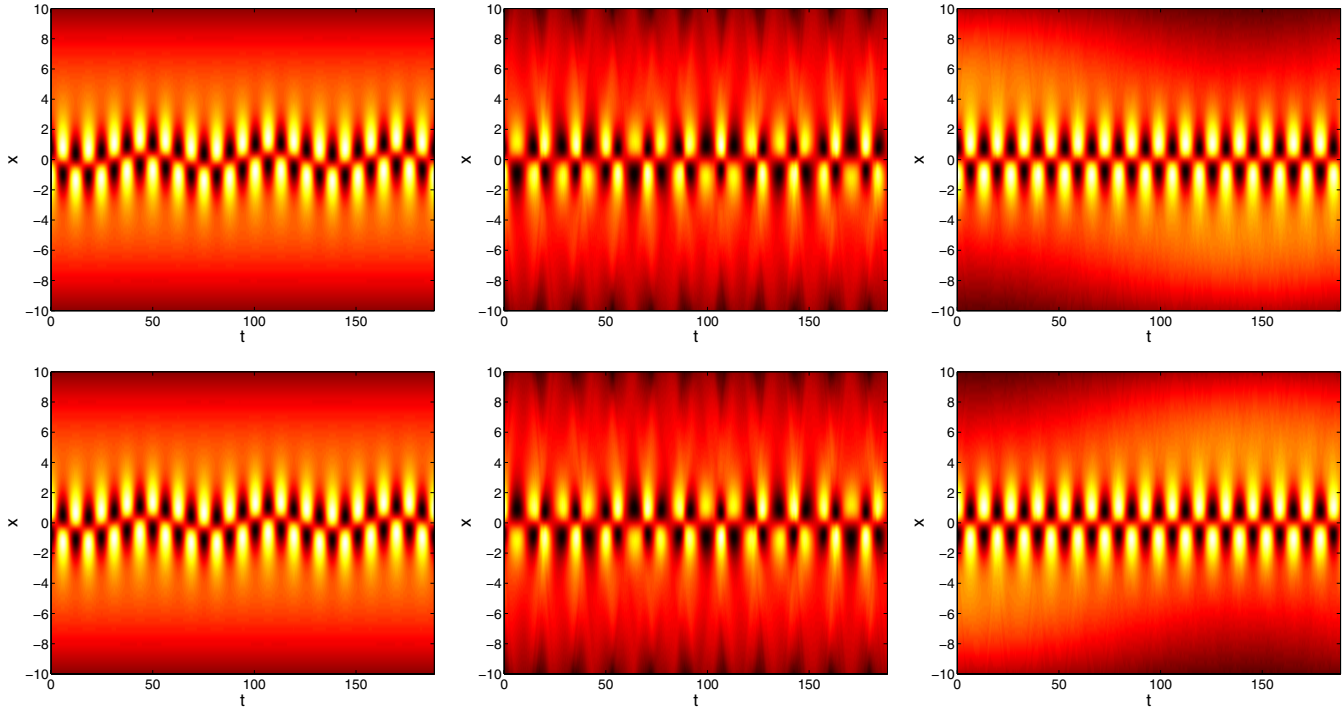

Figure 5. Contour plots showing the evolution of the densities of the DD soliton components (first and second rows depict respective components) when perturbed by three different eigenmodes: the left panel corresponds to a soliton perturbed along the blue mode and leads the soliton to harmonically oscillate near the centre of the trap; in the central panel, the perturbation (along the black mode) leads to a breathing of the soliton width, whereas in the right panel (perturbation along the green mode), the outcome corresponds to an oscillation of the whole condensate. In all cases, $\mu = 3$, $\omega_0 = 0.5$ and $\Omega = 0.2$.

the internal mode corresponding to the oscillation of the trap with respect to ω_0 for fixed $\mu = 5$ and compares it with the frequency predicted by equation (22).

We note here, as an aside in the case $\Omega = 0$, that the internal soliton modes are neutral modes located at $(1, 0)$ on the unit circle. In particular, the mode associated with the oscillation of the DD soliton in the trap becomes in this case a neutral mode associated with the translation of the soliton. The algebraic multiplicity of the multiplier at $(1, 0)$ in the case of $\Omega = 0$ is 8, while in the trapped case (due to the lifting of translational invariance) it is 6.

In order to observe the properties of other internal modes, we have perturbed the beating DD soliton with the corresponding eigenmodes. In particular, a perturbation along the direction of the localized mode depicted in black in the left panel of figure 4 leads to a breathing in the width of the soliton—see the middle panels of figure 5. On the other hand, a perturbation along the direction of the mode depicted in green in the left panel of figure 4 leads to an oscillation

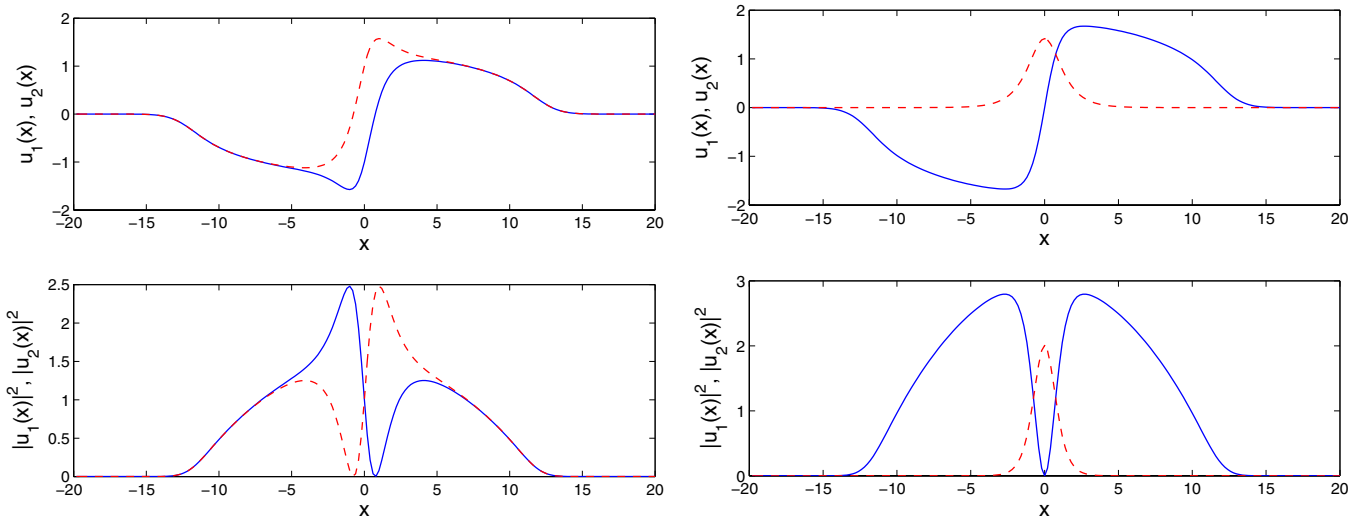

Figure 6. Left panel: profiles and densities of a periodic orbit at $t = 0$ with $\mu = 3$, $\omega_0 = 0.5$ and $\Omega = 0.2$. The right panel shows the DB soliton arising by rotating with $\chi = -\pi/4$ the DD soliton of the left panel.

of the condensate along the trap, leaving the beating DD soliton unaffected (i.e. the soliton stays at the trap centre)—see the right panels of figure 5. For progressively weaker traps, the modes of the background condensate and of the DB solitary wave essentially decouple and in fact two of the frequencies shown in figure 4 (green and blue) tend to 0, as the corresponding motions (of the solitary wave through the background or of the background through the solitary wave) become neutral.

Finally, we make a remark about the way we have calculated the value N_B that must be introduced in equation (22). The procedure consists of performing an $SO(2)$ rotation with $\chi = -\pi/4$ to the periodic DD soliton at $t = 0$. This solution is shown in the left panel of figure 6, whereas the rotated solution is depicted in the right panel of the same figure. Thus, N_B is the norm of the bright component of the rotated solution.

4. Single-beating DD solitons near and far from the Manakov limit

We now turn to a numerical study of the properties of the beating DD soliton states. Firstly, in the absence of a trap, we are going to compare the integrable case with equal scattering lengths $g_{11} : g_{12} : g_{22} = 1 : 1 : 1$ to the non-integrable case $g_{11} : g_{12} : g_{22} = 1.03 : 1 : 0.97$ (see [30]). From figure 7, we observe that both of the dark components are oscillating with fixed frequencies and these two cases are very similar[7]. All of the runs reported below for one of these parameter sets have been repeated with the second one, and in all cases we have observed a close similarity between the dynamical phenomenology of these two cases.

To highlight the fact that substantial variations of the scattering length—which can be imposed by virtue of a Feshbach resonance—may have a significant impact on the

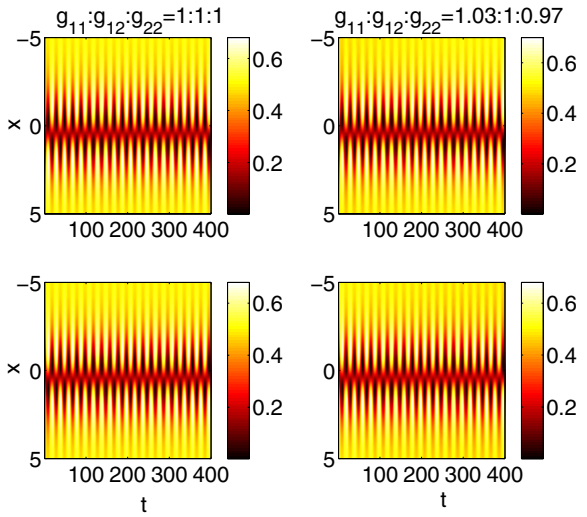

Figure 7. The comparison between the integrable case $g_{11} : g_{12} : g_{22} = 1 : 1 : 1$ (left column) and the non-integrable case $g_{11} : g_{12} : g_{22} = 1.03 : 1 : 0.97$ (right column) is demonstrated. The upper panels show the densities of the first-dark soliton component while the lower ones show the second-dark component. Here $\eta = 0.6$, $\chi = \pi/4$, $\theta = 0$, $k = 0$, $\mu = 1$. Based on the similarity of the relevant dynamics, we will focus on the case of unit nonlinear coefficients.

robustness of the beating DD solitons, we consider scattering lengths in the set with ratios $g_{11} : g_{12} : g_{22} = g : 1 : 1$. In particular, we take $g = 1.1, 1.2, 1.6$ in figure 8. When g is not so large, i.e. $g = 1.1, 1.2$, the beating DD soliton oscillates and, as t increases, the change in the scattering length results in mobility of the coherent structure. However, more dramatic events can arise when g is relatively large, e.g., for $g = 1.6$. There, we can see that the soliton is finally split into two fragments (upon growth of the intrinsic beating oscillation which eventually induces the splitting) and results in two states that resemble dark–anti-dark solitons [31] (see also [29]). In particular, each of the components acquires a dark soliton

[7] In what follows when the relevant interaction coefficients are not explicitly mentioned, it will be implied that they assume the values $g_{11} = g_{12} = g_{22} = 1$.

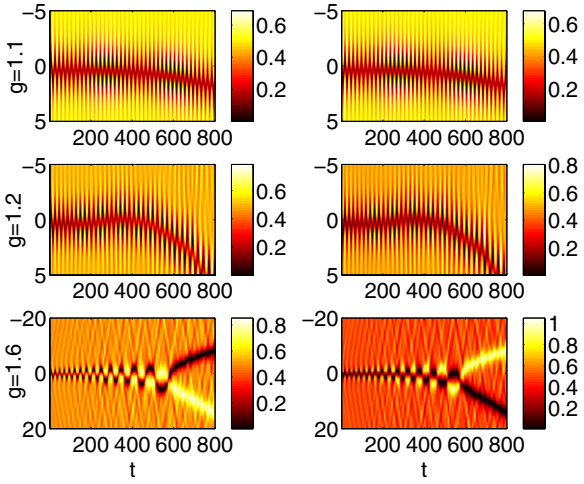

Figure 8. The dynamics of the densities of a DD soliton in the absence of a trap but for $g = 1.1$, $g = 1.2$, $g = 1.6$ respectively ($g \equiv g_{11}$); left and right panels show the densities of the first- and second-dark soliton components, respectively. When $g = 1.1$ or $g = 1.2$, the soliton is set into translational motion. However, for $g = 1.6$ the coherent structure executes a growing oscillation which eventually results in its splitting into a pair of dark–anti-dark solitons (i.e. a dark soliton in one component coupled to a lump in the other). The parameters used here are the same as in figure 7.

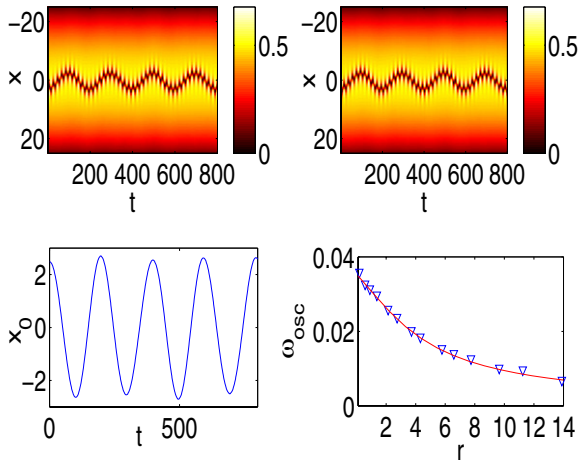

Figure 9. Motion of a DD soliton in a trap of strength $\Omega = 0.05$. Other parameters are the same as in figure 7. The upper two panels show the oscillation of the soliton initially centred at $x_0 = 2.5$ (the chemical potential is $\mu = 1$). The lower left panel demonstrates the centre of mass of the DD in the upper panels. The analytical oscillation frequency, given by equation (22), is 0.03123, while the numerical frequency, calculated by Fourier transform, is 0.03238. The lower right panel yields the comparison between the analytically calculated frequencies (red line) versus the numerical obtained ones (the blue triangles), as r varies between 0.1 and 14.

coupled to an anti-dark soliton, i.e. a density hump (instead of a dip) on top of a finite background, in the second component.

In figure 9, we show a particular example of the DD soliton in the trap, which oscillates around its centre; the parameter values are $\mu = 1$, $\eta = 0.6$, initial soliton position $x_0(t = 0) = 2.5$ and trap strength $\Omega = 0.05$. Note that for these runs, the initial profile of the beating DD soliton in

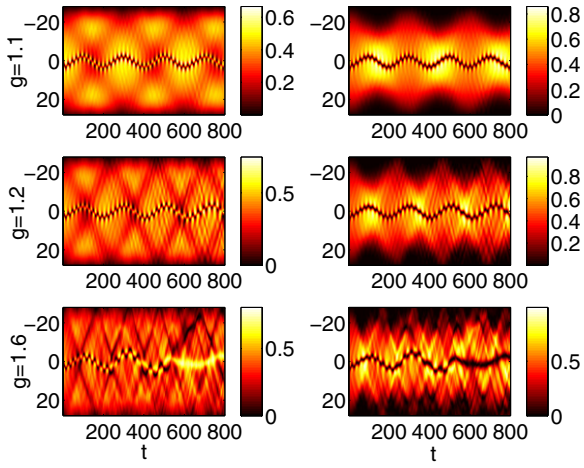

Figure 10. The comparison of the oscillation of the density of a DD soliton within a trap of trap frequency $\Omega = 0.05$ for different values of g; left and right panels depict the first and second component, respectively. The soliton is initialized at $x_0 = 2.5$; g is set to be 1.1 (top panels), 1.2 (middle panels), 1.6 (bottom panels) for the combination of the scattering length $g_{11} : g_{12} : g_{22} = g : 1 : 1$. Other parameters are similar to those in figure 9.

the trap is approximated by the numerically found (in trap) ground state—i.e. the Thomas–Fermi cloud—multiplied by the beating DD solution (without a trap) of equations (13, 14). Then via a time-stepping algorithm (a fourth-order Runge–Kutta scheme), we obtain the time evolution of the densities of the oscillating solitons in the upper two panels. Moreover, the lower-left panel shows the centre of mass of the beating DD soliton in the trap. Using Fourier analysis, we can infer the numerical frequency of in-trap oscillation, which can, in turn, be compared to the analytical one, cf equation (22). As shown in the bottom-right panel of the figure, there is a very good agreement between the two.

Next, we consider the in-trap dynamics of a single-beating DD soliton but for the non-integrable cases. Again, when $g_{11} : g_{12} : g_{22} = 1.03 : 1 : 0.97$, we observe a nearly identical phenomenology to that of unit g_{ij}s. For the more significant deviations from that case of the form $g_{11} : g_{12} : g_{22} = g : 1 : 1$ where $g = 1.1, 1.2, 1.6$, the results are reported in figure 10. For lower values of $g = 1.1, 1.2$, the behaviour of the DD is similar to the case with $g = 1$; however, we progressively observe more significant radiative emissions which also affect the oscillation frequency. However, once again the modifications of the phenomenology are most dramatic in the case of $g = 1.6$ of the bottom panels. There, the radiation emission is accompanied by growing intrinsic oscillations which eventually result in the breakup and formation of a single dark–anti-dark solitary wave.

5. Two DD soliton states: dynamics and interactions

We now consider the interactions of two-beating DD solitons. We once again start from the untrapped case and use as an initial ansatz a two-DB soliton state of the form

$$u_1 = (\cos\phi \tanh\xi_- + \mathrm{i}\sin\phi)(\cos\phi \tanh\xi_+ - \mathrm{i}\sin\phi), \quad (33)$$

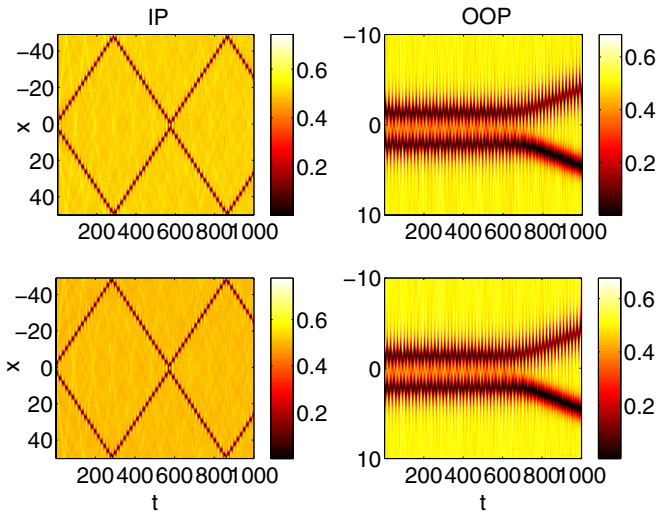

Figure 11. Space–time contour plots of two-beating DD soliton densities in-phase (left) and out-of-phase (right) for $g_{11} = g_{12} = g_{22} = 1$. Here $\chi = \pi/4$, $\eta = 0.5$, $x_0 = 1.5$, $D = 1.2$.

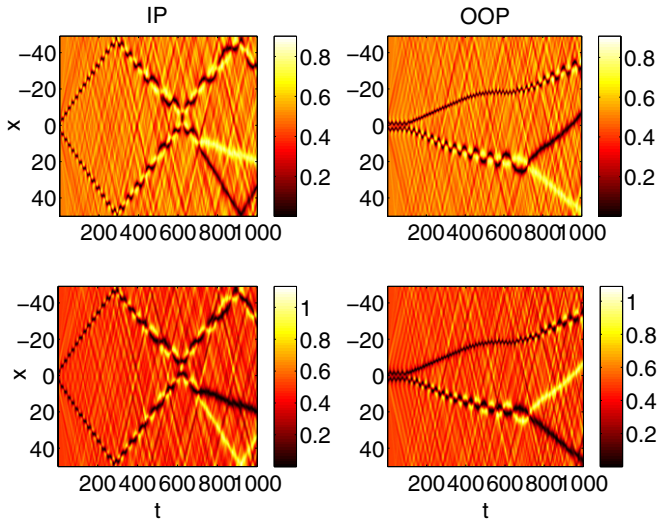

Figure 12. Space–time contour plots of two DD soliton densities in-phase (left) and out-of-phase (right) for $g = 1.6$ in the set $g_{11} : g_{12} : g_{22} = 1.6 : 1 : 1$. Here $\chi = \pi/4$, $\eta = 0.5$, $x_0 = 1.5$, $D = 1.2$.

$$u_2 = \eta \,\mathrm{sech}\,\xi_- \mathrm{e}^{\mathrm{i}\,(kx+\theta(t))} + \mathrm{e}^{\mathrm{i}\,\Delta\theta}\eta \,\mathrm{sech}\,\xi_+ \mathrm{e}^{\mathrm{i}\,(-kx+\theta(t))}, \tag{34}$$

where $\xi_\pm = D(x \pm x_0)$, $2x_0$ is the relative distance between the two solitons and $\Delta\theta$ is the relative phase between the two bright solitons. Below we consider both the out-of-phase (OOP) case, $\Delta\theta = \pi$, as well as the in-phase (IP) case $\Delta\theta = 0$. Once again taking advantage of the model invariance under the $SO(2)$ rotations, as we did for the single-DD soliton case, we use the orthogonal matrix (12) and obtain a two-beating DD soliton *ansatz* in the form

$$\begin{aligned} u_1 = {} & \cos(\chi)\,(\cos\phi\tanh\xi_- + \mathrm{i}\,\sin\phi)\,(\cos\phi\tanh\xi_+ - \mathrm{i}\,\sin\phi) \\ & - \sin(\chi)(\eta\,\mathrm{sech}\,\xi_-\mathrm{e}^{\mathrm{i}\,(kx+\theta(t))} + \mathrm{e}^{\mathrm{i}\,\Delta\theta}\eta\,\mathrm{sech}\,\xi_+ \\ & \times \mathrm{e}^{\mathrm{i}\,(-kx+\theta(t))}), \end{aligned} \tag{35}$$

$$\begin{aligned} u_2 = {} & \sin(\chi)\,(\cos\phi\tanh\xi_- + \mathrm{i}\,\sin\phi)\,(\cos\phi\tanh\xi_+ - \mathrm{i}\,\sin\phi) \\ & + \cos(\chi)(\eta\,\mathrm{sech}\,\xi_-\mathrm{e}^{\mathrm{i}\,(kx+\theta(t))} + \mathrm{e}^{\mathrm{i}\,\Delta\theta}\eta\,\mathrm{sech}\,\xi_+ \\ & \times \mathrm{e}^{\mathrm{i}\,(-kx+\theta(t))}). \end{aligned} \tag{36}$$

In our numerical study for the dynamics of the two-beating DD soliton state, we first consider the integrable case, corresponding to $g_{11} = g_{12} = g_{22} = 1$, both for the IP and OOP cases. The results of the simulations, using initial conditions corresponding to the above ansatz, are shown in figure 11. In the IP case, the repulsion between the beating DD solitons is immediately evident resulting in the strong separation of the two waves (which still perform their internal beating). On the other hand, in the OOP case, the competition between the repulsion of the dark components and the attraction between the bright components of the progenitor DB solitons (see [32]) can be discerned, as the configuration remains nearly stationary for a lengthy evolution interval. Finally, however, the repulsive interaction prevails and the solitons eventually separate.

Next, we consider the non-integrable case. Since for $g_{11} : g_{12} : g_{22} = 1.03 : 1 : 0.97$, the phenomenology is again very similar to $g_{11} = g_{12} = g_{22}$, we consider the significant departure from this limit pertaining to $g_{11} : g_{12} : g_{22} = 1.6 : 1 : 1$. In figure 12, we observe that in the IP case, the two-beating DD solitons initially separate and move away from each other, then they are reflected from the domain boundary and a new collision occurs. After this collision, a highly non-trivial event is observed, namely one of the two-beating DD solitons is decomposed into a dark–anti-dark soliton pair, with each of these solitons moving with different velocities. It should be pointed out here that the reflection from the domain boundary is a by-product of the no-flux boundary conditions used in the simulations. Nevertheless, we chose to illustrate the evolution for such longer times (instead of truncating it prior to such boundary-induced reflection and subsequent collision) in order to encompass the interesting phenomenology of the collision of the reflected waves and in that light contrast the integrable interaction of figure 11 with the highly non-integrable one of figure 12. For the OOP case, the separation arises much faster than for the unit coefficients and, interestingly, results in an asymmetric evolution with one of the DD solitons breaking up in a pair of dark–anti-dark solitons (as in figure 8 of section 2). Note that, as in the IP case, the other soliton is not broken up in a similar way during the horizon of the simulation, although it is likely that such an event will also occur for that wave.

Next, we consider the two-beating DD soliton in the trap, in the case of unit coefficients. We set $V(x) = \frac{1}{2}\Omega^2 x^2$, with $\Omega = 0.05$, and the chemical potential $\mu = 1$. From figure 13, we infer that the two-beating DD solitons are now trapped and oscillate around an equilibrium position. Note that in the IP case, the solitons perform OOP oscillations and undergo quasi-elastic collisions. In the OOP case, the weak residual repulsion is counter balanced by the presence of the trap, and we observe that the two-beating DD solitons remain in a close distance to each other.

Finally, we consider two DD waves with $g_{11} : g_{12} : g_{22} = 1.6 : 1 : 1$ within the same trap in figure 14. In this case, we

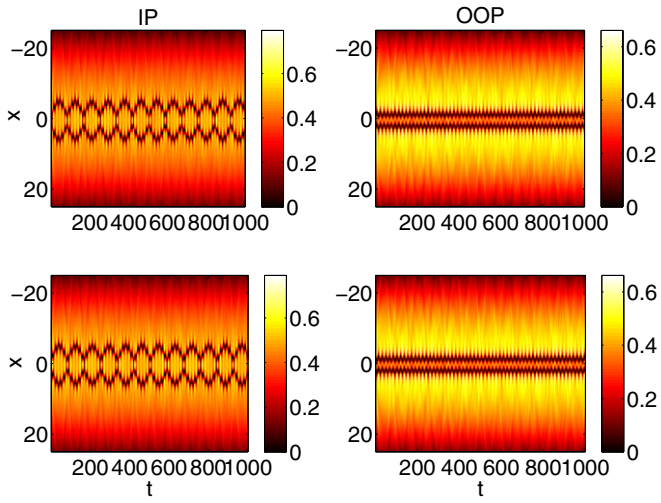

Figure 13. Space–time contour plots of two-beating DD soliton densities in-phase (left) and out-of-phase (right) in the case of equal g_{ij}s within a harmonic trap with trap frequency $\Omega = 0.05$. Here $\chi = \pi/4$, $\eta = 0.5$, $x_0 = 1.5$, $D = 1.2$, $\mu = 1$.

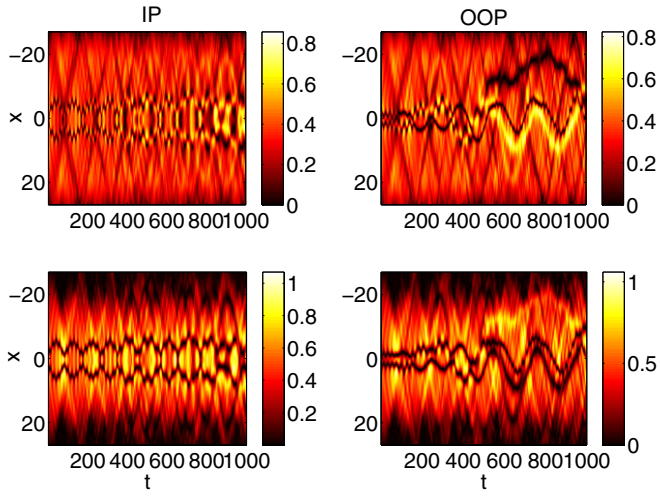

Figure 14. Space–time contour plots of two-beating DD soliton densities in-phase (left) and out-of-phase (right) for the case with $g_{11} : g_{12} : g_{22} = 1.6 : 1 : 1$ within a harmonic trap with trap frequency $\Omega = 0.05$. The parameters used are the same as for the previous figure.

observe that despite the presence of the trap, it is not possible to sustain a robust set of oscillations and interactions between the beating DD solitons. This is especially true in the OOP case, where the oscillatory growth of the beating eventually results in the breakup of the DD soliton states into dark–anti-dark ones (which generally appear more robust for such higher values of g).

6. Conclusions and future challenges

In this work, we have studied the stability and dynamics of beating dark–dark (DD) solitons in pseudo-spinor Bose–Einstein condensates, motivated by recent experiments where such structures were observed. We have illustrated the connection of these solitons with internal density oscillations to dark–bright (DB) solitons identified earlier, through $SO(2)$ (and more generally $SU(2)$) rotations. We have illustrated that such states persist in the presence of the trap and, in fact, oscillate with the frequency previously predicted for DB solitons. Using Floquet analysis, we have also identified beating DD solitons as stable periodic orbits in the integrable (Manakov) limit with and without a trap.

We have also investigated in detail the effect of the deviation from the Manakov case by considering different from unity scattering length ratios. We have shown that when the deviation from the integrable case is small (as is the physically relevant case of a pseudo-spinor condensate composed by different spin states of rubidium), then the stability and dynamics of beating DD solitons follow that of the integrable case. However, we also illustrated that a significant departure of the ratios of the scattering lengths from this limit (towards the miscible regime) will eventually break up beating DD solitons in favour of dark–anti-dark soliton entities. We have also considered the interaction of beating DD solitons finding a typically repulsive dynamical behaviour, which can be attenuated only in the case where the bright components (of the progenitor DB solitons, used to create the DD ones) are out-of-phase (and, hence, attracting each other). In that case, especially in the presence of a trap, a robust set of multiple beating DD soliton states can be created.

The discussion of DD solitons in this work has focused upon those states that can be constructed, in the spatially extended Manakov case, from the $SU(2)$ rotation of a DB soliton and confined states in the presence of a trapping potential. In both cases, each component of the DD soliton exhibits the same background flow velocity. In a series of experiments [18, 25, 19, 32], a relative flow between two condensate components induced by a magnetic field gradient led to DB solitons and counterflow-induced modulational instability resulting in the formation of a number of beating DD solitons. It is natural, then, to inquire into the effect that relative motion between two condensate components has on localized structures. In the integrable case, the most general DD soliton was constructed using a Bäcklund transformation [28]. Because it allows for a counterflow, this soliton is characterized by eight free parameters in contrast to the seven-parameter $SU(2)$-rotated DB soliton studied here or the seven-parameter static DD soliton [36]. However, and since the present study focused predominantly on the five-parameter family stemming from the $SO(2)$ rotation, the persistence, stability, and interactions of the full seven-parameter solitonic states (and even the eight-parameter generalization thereof presented within [28]) in the non-integrable case constitute themes worthy of further study.

There are many other directions that are worth considering further along the lines of this work. Quantifying further (and semi-analytically, if possible) the interactions between the beating DD solitons, as well as studying in more detail the dark–anti-dark solitons that appear to spontaneously arise from their breakup in the miscible regime are interesting extensions of this work in the one-dimensional setting. On the other hand, one naturally may consider the two-dimensional (2D) generalization of the considerations herein, especially upon

bearing in mind that the $SU(2)$ (or $SO(2)$) rotations used herein are not restricted to the one-dimensional realm in any particular way. In that regard, one may envision vortex–bright soliton states [33] (i.e. the 2D analogue of the DB waves) rotated via $SO(2)$ to produce vortex–vortex-type states (in analogy with the DD ones). Such states are currently under study and will be reported in future publications.

Note added in proof. After the submission of this work, Dr A Nicolin informed one of us (PGK) about a recent preprint related to immiscible two-component Bose–Einstein condensates and the Faraday wave patterns that can arise in them. The relevant work has now been published as [37].

Acknowledgments

PGK acknowledges the support from NSF-DMS-0806762 and from the Alexander von Humboldt Foundation. The work of DJF was partially supported by the Special Account for Research Grants of the University of Athens. PE acknowledges support from NSF and ARO. MH acknowledges support from NSF DMS 1008973. JC acknowledges financial support from the MICINN project FIS2008-04848.

References

[1] Kevrekidis P G, Frantzeskakis D J and Carretero-González R 2008 *Emergent Nonlinear Phenomena in Bose–Einstein Condensates: Theory and Experiment* (Heidelberg: Springer)
[2] Carretero-González R, Frantzeskakis D J and Kevrekidis P G 2008 *Nonlinearity* **21** R139
[3] Abdullaev F Kh, Gammal A, Kamchatnov A M and Tomio L 2005 *Int. J. Mod. Phys.* B **19** 3415
[4] Frantzeskakis D J 2010 *J. Phys. A: Math. Theor.* **43** 213001
[5] Burger S, Bongs K, Dettmer S, Ertmer W, Sengstock K, Sanpera A, Shlyapnikov G V and Lewenstein M 1999 *Phys. Rev. Lett.* **83** 5198
[6] Denschlag J *et al* 2000 *Science* **287** 97
[7] Dutton Z, Budde M, Slowe C and Hau L V 2001 *Science* **293** 663
[8] Anderson B P, Haljan P C, Regal C A, Feder D L, Collins L A, Clark C W and Cornell E A 2001 *Phys. Rev. Lett.* **86** 2926
[9] Bongs K, Burger S, Dettmer S, Hellweg D, Arlt J, Ertmer W and Sengstock K 2001 *C. R. Acad. Sci. Paris* **2** 671
[10] Becker C, Stellmer S, Soltan-Panahi P, Dörscher S, Baumert M, Richter E-M, Kronjäger J, Bongs K and Sengstock K 2008 *Nature Phys.* **4** 496
[11] Stellmer S, Becker C, Soltan-Panahi P, Richter E-M, Dörscher S, Baumert M, Kronjäger J, Bongs K and Sengstock K 2008 *Phys. Rev. Lett.* **101** 120406
[12] Shomroni I, Lahoud E, Levy S and Steinhauer J 2009 *Nature Phys.* **5** 193
[13] Weller A, Ronzheimer J P, Gross C, Esteve J, Oberthaler M K, Frantzeskakis D J, Theocharis G and Kevrekidis P G 2008 *Phys. Rev. Lett.* **101** 130401
[14] Theocharis G, Weller A, Ronzheimer J P, Gross C, Oberthaler M K, Kevrekidis P G and Frantzeskakis D J 2010 *Phys. Rev.* A **81** 063604
[15] Engels P and Atherton C 2007 *Phys. Rev. Lett.* **99** 160405
[16] Busch Th and Anglin J R 2001 *Phys. Rev. Lett.* **87** 010401
[17] Nistazakis H E, Frantzeskakis D J, Kevrekidis P G, Malomed B A and Carretero-González R 2008 *Phys. Rev.* A **77** 033612
[18] Hamner C, Chang J J, Engels P and Hoefer M A 2011 *Phys. Rev. Lett.* **106** 065302
[19] Hoefer M A, Hamner C, Chang J J and Engels P 2011 *Phys. Rev.* A **84** 041605
[20] Chen Z, Segev M, Coskun T H, Christodoulides D N, Kivshar Yu S and Afanasjev V V 1996 *Opt. Lett.* **21** 1821
Chen Z, Segev M, Coskun T, Christodoulides D N and Kivshar Yu S 1997 *J. Opt. Soc. Am.* B **14** 3066
[21] Ostrovskaya E A, Kivshar Yu S, Chen Z and Segev M 1999 *Opt. Lett.* **24** 327
[22] Rajendran S, Muruganandam P and Lakshmanan M 2009 *J. Phys. B: At. Mol. Opt. Phys.* **42** 145307
[23] Yin C, Berloff N G, Pérez-García V M, Novoa D, Carpentier A V and Michinel H 2011 *Phys. Rev.* A **83** 051605
[24] Álvarez A, Cuevas J, Romero F R and Kevrekidis P G 2011 *Physica* D **240** 767
[25] Middelkamp S, Chang J J, Hamner C, Carretero-González R, Kevrekidis P G, Achilleos V, Frantzeskakis D J, Schmelcher P and Engels P 2011 *Phys. Lett.* A **375** 642
[26] Yan D, Chang J J, Hamner C, Kevrekidis P G, Engels P, Achilleos V, Frantzeskakis D J, Carretero-González R and Schmelcher P 2011 *Phys. Rev.* A **84** 053630
[27] Achilleos V, Kevrekidis P G, Rothos V M and Frantzeskakis D J 2011 *Phys. Rev.* A **84** 053626
[28] Park Q-H and Shin H J 2000 *Phys. Rev.* E **61** 3093
[29] Susanto H, Kevrekidis P G, Carretero-González R, Malomed B A, Frantzeskakis D J and Bishop A R 2007 *Phys. Rev.* A **75** 055601
[30] Mertes K M, Merrill J, Carretero-González R, Frantzeskakis D J, Kevrekidis P G and Hall D S 2007 *Phys. Rev. Lett.* **99** 190402
[31] Kevrekidis P G, Nistazakis H E, Frantzeskakis D J, Malomed B A and Carretero-González R 2004 *Eur. Phys. J.* D **28** 181
[32] Yan D, Chang J J, Hamner C, Kevrekidis P G, Engels P, Achilleos V, Frantzeskakis D J, Carretero-González R and Schmelcher P 2011 arXiv:1104.4359
[33] Law K J H, Kevrekidis P G and Tuckerman L S 2010 *Phys. Rev. Lett.* **105** 160405
[34] Susanto H, Cuevas J and Krüger P 2011 *J. Phys. B: At. Mol. Opt. Phys.* **44** 095003
[35] Melvin T R O, Champneys A R, Kevrekidis P G and Cuevas J 2008 *Physica* D **237** 551
[36] Sheppard A P and Kivshar Y S 1997 *Phys. Rev.* E **55** 4773
[37] Balaž A and Nicolin A I 2012 *Phys. Rev.* A **85** 023613